EVOLUTION AND ERUPTION OF GEOTHERMALLY COOLED MAGMA BODIES

David Dempsey[1], Darren Gravley[2], Julie Rowland[3]

[1]Department of Engineering Science, University of Auckland, Auckland, New Zealand

[2]Department of Geological Sciences, University of Canterbury, Christchurch, New Zealand

[3]School of Environment, University of Auckland, Auckland, New Zealand

d.dempsey@auckland.ac.nz

Keywords: *magma body, eruption, geothermal system, model, magmatic fluids, viscoelastic*

ABSTRACT

Magmatic geothermal systems extract heat and volatiles from deep magma bodies and transport these upward through the brittle crust. Sometimes, these same magma bodies evolve toward an unstable, overpressured state, precipitating a catastrophic caldera eruption. Understanding the deep coupling between magmatic and geothermal systems can help contextualise our near surface observations and plan for utilisation of the deep resource. In addition, insight into how the system transitions between convective and eruptive phases has implications for our understanding of volcanic hazard.

Here, we introduce a lumped parameter thermomechanical model of a magma body that is being cooled from above by geothermal systems, and recharged from below by deep magma sources. The model tracks the evolution of temperature, pressure and magma composition, and includes parameterised descriptions of eruption, volatile leakage across a viscoelastic shell, and overlying geothermal systems. We have used this model to explore generic eruptive styles and to develop an approximation of the eruptive record of the modern Taupō Volcanic Zone (TVZ).

Our findings suggest that magma bodies at 4 to 5 km depth in the TVZ are overlaid by a 500 m thick, high-temperature, partly permeable (10^{-19} -10^{-20} m^2), viscoelastic shell. The timing and volume of eruptions are dominated by short intervals of sporadic magma recharge originating deeper in the crust. Long-term climatic modulation of rainfall driven geothermal systems has minimal impact on eruptive timing. However, under certain conditions, efficient geothermal systems can trigger an eruption by cooling a magma body too rapidly, resulting in gas exsolution that builds to a critical overpressure. These insights highlight the value of coupled magmatic-geothermal models, and suggest development of a magmatic reservoir simulator could shine new light on the complex physical interplays occurring deep in the TVZ.

1. INTRODUCTION

Geothermal systems scattered throughout the Taupō Volcanic Zone (TVZ) are the uppermost manifestation of a vast lithospheric heat transport system. Convecting groundwater percolates downward through the brittle crust, becoming heated from contact with magmatic intrusions as deep as 8 km. Some of these intrusions, such as the one drilled at 2.5 km depth beneath Ngatamariki (*Arehart et al.,* 2002), exist in a solid, non-eruptible state. However, the extensive eruptive history of the TVZ – at least 21 eruptions from the Taupō and Okataina calderas since 30ka (*Lowe et al.*, 2013) – indicates that, in the past, others must have existed at shallow depths in a melt-dominated, eruptible state. The geothermal-magmatic interaction is also identified by geochemical studies (*Giggenbach*, 1995; *Bégué et al.*, 2017) that indicate there may be up to 20 wt % of magmatic volatiles in TVZ geothermal waters.

As meteoric water is heated during its long journey through the crust, both its density and viscosity are changed. Indeed, the decrease in density at high temperature provides the underlying impetus that drives a geothermal system's buoyant upflow. In a similar manner, when a deep magma body gains or loses heat, its internal properties will change, influencing its potential for eruption (Fig. 1). For instance, cooling of molten rock increases the volume fraction of condensed crystals (the solid), which, being denser than the

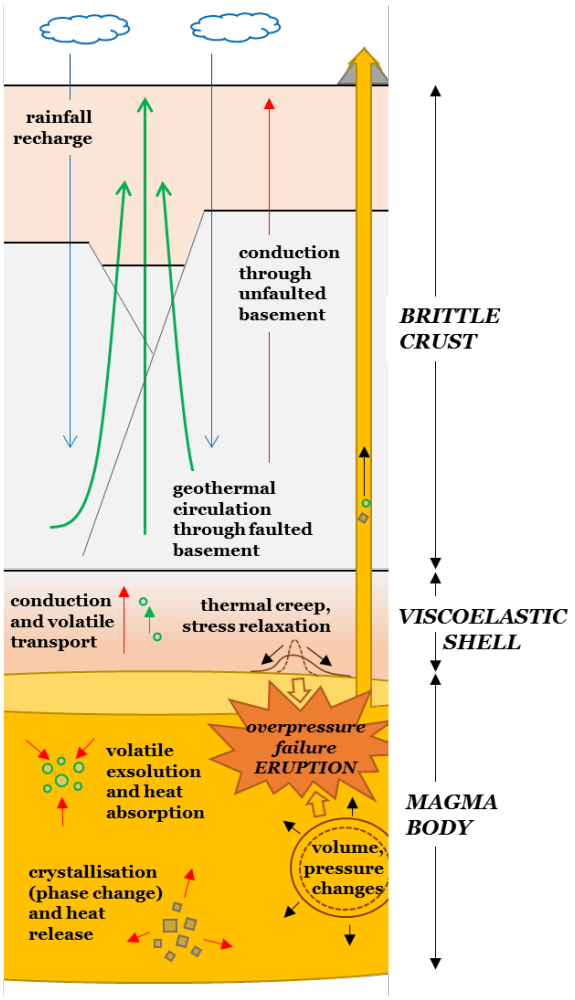

Figure 1: Schematic showing the key physics governing magma body evolution and its interaction with overlying geothermal systems.

melt, reduces overpressure, and hence eruptibility. However, at the same time, gas volatiles (H_2O, CO_2, Cl) that were dissolved in the melt phase, are exsolved to coexist alongside the crystal-melt mixture. This increases overpressure and induces stresses in the rock surrounding the magma body. If the stresses are sufficiently large, a dike can propagate to the surface, triggering an eruption. If not, ductile creep in the high-temperature zone around the magma body will slowly dissipate these stresses.

To model a coupled magma body-geothermal system we need to link a range of conservation (mass, water, energy, momentum) and constitutive laws (viscoelasticity, phase change, Darcy flow). Such a formulation introduces a large number of parameters, many of which are poorly constrained. Nevertheless, these models can still help us to understand and rank competing physics, and to begin exploring unanswered questions. How do magmatic fluids travel through extremely high temperature (>350°C) ductile rock to become entrained in a geothermal system? What controls the triggering of eruptions? What role do TVZ geothermal systems play in suppressing or enhancing these?

2. MODEL DEVELOPMENT

The model developed here is a modification of the silicic magma chamber model presented by *Degruyter and Huber* (2014), hereafter D&H. Those authors used their model to study eruption triggers and frequency in spherical magma bodies. The principle differences between the D&H model and the one we present here are: (1) coupling to a rainfall-driven geothermal heat transport model; (2) consideration of volatile transport across a permeable viscoelastic shell; and (3) consideration of a sill geometry for the magma body.

2.1 Magma body evolution

Following the approach of D&H, we conceptualise a magma body as a well-mixed composition of melt (liquid rock), crystals (solid rock) and an exsolved volatile phase (supercritical water). The magma body has pressure, P, temperature, T, and volume, V, whose time evolution we seek to model. The mixture is characterised by the volume fractions for melt, ϵ_m, crystals, ϵ_X, and exsolved water, ϵ_g, which satisfy the closure condition:

$$\epsilon_m + \epsilon_X + \epsilon_g = 1. \tag{1}$$

Each component has its own density, which evolves with the magma body. The mixture density, ρ, is given:

$$\rho = \epsilon_m\rho_m + \epsilon_X\rho_X + \epsilon_g\rho_g, \tag{2}$$

where equations of state are prescribed for water density, $\rho_g(P,T)$, and melting, $\epsilon_X(T,\epsilon_g)$ (Appendix A). Taking these, along with Eq. (1), there are three additional variables – ϵ_g, ρ_m and ρ_X – whose evolution must be determined by the model. The two rock densities are presumed to vary with pressure and temperature only:

$$\frac{d\rho_m}{dt} = \frac{1}{\beta_m}\frac{dP}{dt} - \alpha_m\frac{dT}{dt}, \tag{3}$$

$$\frac{d\rho_X}{dt} = \frac{1}{\beta_X}\frac{dP}{dt} - \alpha_X\frac{dT}{dt}, \tag{4}$$

where β_i and α_i are, respectively, bulk moduli and coefficients of thermal expansion.

Conservation of total mass, $M = \rho V$, is expressed:

$$\rho\frac{dV}{dt} + \frac{d\rho}{dt}V = \dot{M}_{in} - \dot{M}_{erupt} - \dot{M}_{w,leak}, \tag{5}$$

where $\dot{M}_{in}$ is recharging magma from a deeper source. In the D&H model, $\dot{M}_{erupt}$ represents sporadic eruption from the magma body, i.e., it is zero at all time except during short periods when eruption conditions are satisfied. Here, we have included an additional term, $\dot{M}_{w,leak}$, which represents the continuous loss of water across a leaky viscoelastic shell.

Volume changes of the reservoir are driven by the elastic response to overpressure, thermal expansion, and viscoelastic creep:

$$\frac{1}{V}\frac{dV}{dt} = \frac{1}{\beta_r}\frac{dP}{dt} + \frac{\Delta P}{\eta_r} - \alpha_r\frac{dT}{dt}, \tag{6}$$

where η_r is the effective viscosity of the high-temperature, viscoelastic shell that surrounds the magma body, and $\Delta P = P - P_{lith}$ is the overpressure (pressure above lithostatic). Combining Eqs. (2), (5) and (6), we express the governing equation for mass conservation:

$$A_m\frac{dP}{dt} + B_m\frac{dT}{dt} + C_m\frac{d\epsilon_g}{dt} + D_m = 0, \tag{7}$$

where the coefficients $A_m \ldots D_m$ are given in Appendix A.

Conservation of the total mass of dissolved and exsolved water, M_w, is expressed:

$$\frac{dM_w}{dt} = \dot{M}_{w,in} - \dot{M}_{w,erupt} - \dot{M}_{w,leak}, \tag{8}$$

$$M_w = \epsilon_g\rho_g V + m_{eq}\epsilon_m\rho_m V, \tag{9}$$

where $m_{eq}(P,T)$ is the equilibrium dissolved water content in the melt, an equation of state given in Appendix A. Incoming water is assumed to be completely dissolved in the incoming melt, and $\dot{M}_{w,erupt}$ is the component of $\dot{M}_{erupt}$ lost as water during periodic eruptions, assumed to be in proportion with the exsolved and dissolved water in the magma body. Combining Eqs. (2), (6), (8) and (9), we express the governing equation for water conservation:

$$A_w\frac{dP}{dt} + B_w\frac{dT}{dt} + C_w\frac{d\epsilon_g}{dt} + D_w = 0, \tag{10}$$

where the coefficients $A_w \ldots D_w$ are given in Appendix A.

Conservation of enthalpy, H, is expressed:

$$\frac{dH}{dt} = \dot{H}_{in} - \dot{H}_{erupt} - \dot{H}_{cool} - \dot{H}_{leak}, \tag{11}$$

where the incoming enthalpy is $\dot{H}_{in} = c_{in}T_{in}\dot{M}_{in}$, and c_{in} and T_{in} are the specific heat and temperature of recharging magma mixture. Enthalpy loss comprises three components (Fig. 1): (i) enthalpy of the erupted mass, $\dot{H}_{erupt}$; (ii) enthalpy lost by conductive cooling through the viscoelastic shell, $\dot{H}_{cool}$; and (iii) enthalpy lost by leaking fluids, $\dot{H}_{leak}$.

Enthalpy of the magma body is comprised of sensible heat, latent heat of crystallisation, L_m, and exsolution, L_e:

$$H = \rho cTV - L_m\rho_X\epsilon_X V - L_e m_{eq}\rho_m\epsilon_m V, \tag{12}$$

where c is the specific heat of the mixture:

$$c = \frac{1}{\rho}\left(\epsilon_X\rho_X c_X + \epsilon_m\rho_m c_m + \epsilon_g\rho_g c_g\right). \tag{13}$$

Combining Eqs. (2), (6), (11), (12) and (13), we express the governing equation for enthalpy conservation:

$$A_h \frac{dP}{dt} + B_h \frac{dT}{dt} + C_h \frac{d\epsilon_g}{dt} + D_h = 0, \qquad (14)$$

where the coefficients $A_h \ldots D_h$ are given in Appendix A.

Eqs. (7), (10) and (14), which together express the coupled evolution of P, T and ϵ_g, are inverted by Cramer's rule to obtain individual evolution equations. These are solved, along with Eqs. (3), (4) and (6), using an implicit Runge-Kutta method implemented in the Python function `scipy.integrate.solve_ivp`. The integrator solves up to specific events – in our case, onset or cessation of an eruption – at which time model parameters (e.g., $\dot{M}_{erupt}$) or time-stepping can be modified.

The condition for an eruption to occur is:

$$\Delta P > \min(\Delta P_{cd}, \Delta P_{cf}) \quad \text{and} \quad \epsilon_X < 0.5, \qquad (15)$$

where ΔP_{cd} is the critical overpressure required to propagate a viscous dike to the surface, initiating an eruption (*Jellinek and DePaolo*, 2003), and ΔP_{cf} is the critical overpressure for fragmentation (*Spieler et al.*, 2004). The second condition on crystallinity expresses a mobility requirement: when the solid fraction exceeds 50%, the magma locks up and can no longer flow. Hence, it is non-eruptible.

An eruption halts when overpressure has been dissipated or the magma body becomes locked:

$$\Delta P \leq 0 \quad \text{or} \quad \epsilon_X > 0.5. \qquad (16)$$

2.2 Geothermal model

In the D&H model, the conductive cooling rate, $\dot{H}_{cool}$, is computed from an approximation of an evolving radial temperature distribution inside a viscoelastic shell that surrounds the spherical magma body. In the D&H model, η_r was calculated using a thermally activated Arrhenius law, $\eta_r = A_D \exp(G/RT)$, where A_D, G and R are constants and T is the average temperature in the shell. Here, we prescribe a fixed value for η_r.

In a departure from the D&H model, we assume the magma body has a sill geometry, whose upper surface is at a depth, z_{mb}. For this geometry, V can be expressed as the product of lateral area, A, and thickness, Δz. We retain the assumption of a well-mixed magmatic composition, although as a magma body becomes increasingly stretched, lateral heterogeneities could become significant.

We further assume that the *dominant* component of $\dot{H}_{cool}$ is driven by geothermal systems that form in the brittle crust overlying the magma body. Although these systems do not directly contact the magma body, we suggest that they do cool the upper crust to such an extent that the depth of the brittle-ductile transition, z_{BDT}, as delineated by the 350°C isotherm, is deeper than it would be in a purely conductive regime (Fig. 2). This allows for a non-arbitrary definition of two heat transporting zones above the magma body: (i) a low-permeability ductile zone of dominantly conductive heat flow across steep temperature gradients; overlaid by (ii) a brittle zone hosting geothermal convection in zones of elevated fracture permeability, and a minor component of conductive heat flow elsewhere. If the average geothermal heat transported per unit area of magma body is W, then, at steady state, heat flow is the same through both zones:

$$K \frac{T - T_{BDT}}{z_{mb} - z_{BDT}} = W + K \frac{T_{BDT} - T_{atm}}{z_{BDT}}, \qquad (17)$$

where K is the thermal conductivity, and T_{atm} is atmospheric temperature. This model assumes that lateral and downward heat conduction out of the magma body can be neglected because these are small compared to the upward, geothermally enhanced conduction.

The purpose of formulating Eq. (17) is to estimate the depth to the brittle-ductile transition, z_{BDT}, and hence the thickness of the viscoelastic layer. One way to do this is to express W as some multiple, γ, of the conductive heat flow in the brittle layer (second term on the RHS of (17)). In which case:

$$z_{BDT} = z_{mb} \left(1 + \frac{(T - T_{BDT})}{(1+\gamma)(T_{BDT} - T_{atm})} \right)^{-1} \qquad (18)$$

Hochstein (1995) constructed a heat budget for the TVZ and estimated the anomalous conductive (<50 MW per 100 km) and geothermal heat flows (between 1500 and 2000 MW per 100 km), which could put γ in the range 30 to 40. However, Hochstein's estimate of the conductive heat flow is likely low, as it was limited to non-geothermal areas at the margins of the TVZ. An upper bound is constructed by computing the total conductive flux across a 100×25 km strip of TVZ, assuming an average z_{BDT} of 6 km (*Bryan et al.*, 1999) and $K = 2.5$ W m^{-2} K^{-1}, about 340 MW. In this case, γ could be as low as 4.5. For an 800°C magma body at a depth of 4 km, an intermediate $\gamma = 10$ and $T_{atm} = 25$°C, Eq. (18) suggests the viscoelastic zone should be about 450 m thick.

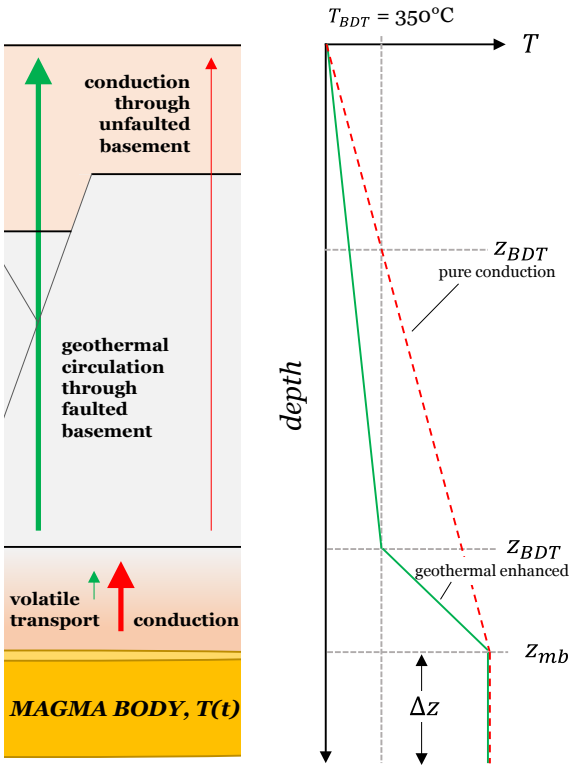

Figure 2: Schematic of conceptualized crustal heat transfer zones overlying a magma body and corresponding conductive temperature profiles (i.e., outside the upflow of a geothermal system).

Given an estimate of z_{BDT}, the geothermally enhanced conductive heat loss through the viscoelastic shell is:

$$\dot{H}_{cool} = AK\frac{T - T_{BDT}}{z_{mb} - z_{BDT}}. \quad (19)$$

Eq. (18) suggests that the depth to the brittle ductile transition is governed by the competition between geothermal power, parameterised by γ, and magmatic thermal potential, characterised by T. The concept of BDT depth depression due to geothermal circulation has been previously explored by *Kissling et al.* (2009). In that study, permeability was reduced by a factor dependent on a thermally activated viscoplastic rheology, i.e., permeability evolved alongside temperature. In a follow-up study, *Kissling and Ellis* (2011) coupled their geothermal model to a larger-scale lithospheric rifting model that predicted fault and partial melt formation. Both studies indicated that localisation of geothermal systems depended on dynamic processes at and below the BDT.

In our model, as a magma body cools, the viscoelastic zone above it will thin and hence z_{BDT} will deepen. Conversely, in the event that the heat transfer efficiency of geothermal systems is diminished, then z_{BDT} will progressively shallow and $\dot{H}_{cool}$ will decrease. What could modulate the geothermal heat output, γ, in such a manner?

2.2.1 Rainfall-controlled geothermal fields

Weir (2009) introduced a mathematical model of "once through" geothermal circulation supplied by infiltrating rainwater. Among the many expressions he develops, those for the mass flux rate, q_{fld}, and power output, W_{fld}, for individual fields are particularly relevant:

$$q_{fld} = \rho_d \epsilon \dot{R} \quad (20)$$

$$W_{fld} = h_u q_{fld} A_d \quad (21)$$

where ρ_d is density of the downwelling fluid (1000 kg m^{-3}), A_d is the downflow area, $\dot{R}$ is the regional rainfall rate (~1200 mm yr^{-1}), ϵ is the fraction of rainfall that infiltrates into the groundwater system, and h_u is the upflow enthalpy (~1550 kJ kg^{-1} for liquid water at 350°C at 4-6 km depth). *Dempsey et al.* (2012) showed that TVZ-like geothermal systems focused downwelling water from catchments that were about 7 times larger than the upflowing region, i.e., $A_d \approx 7A_u$ (where A_u is between 5 and 35 km^2 in the TVZ; *Bibby et al*., 1995).

Then, an area, A, can sustain an average of $N_{fld} = 7A/8A_d$ individual geothermal fields, each with a power output, W_{fld}. The geothermal flux through A is then:

$$W = \frac{7}{8} h_u \rho_d \epsilon \dot{R}, \quad (22)$$

which when expressed as a fraction, γ, of the conductive heat flux through A gives:

$$\gamma = \frac{7 h_u \rho_d \epsilon \dot{R} z_{BDT}}{8K(T_{BDT} - T_{atm})}. \quad (23)$$

Kissling and Weir (2005) estimate the infiltration fraction, ϵ, to be about 0.02 for the present day TVZ. This number parameterises all factors that contribute to rainwater infiltration, which presumably includes the bulk permeability of the brittle crust. We speculate that ϵ could respond to changes in the rate of rifting and faulting in the TVZ, however, we are unable to quantify these changes.

Most of the other terms in Eq (23) are fixed by the properties of water (h_u and ρ_d) or rock (T_{BDT} and K). However, the rainfall rate, $\dot{R}$, could potentially vary over climate cycles. For instance, *Eaves et al.* (2016) have suggested that central North Island rainfall could be up to 25% less during periods of glaciation. We note that while, in areas such as Iceland, volcanic activity can be modulated by the growth and retreat of ice sheets (*Sigmundsson et al.*, 2010), no such ice sheets formed in the Central North Island during previous glacial periods.

2.3 Fluid transport across the viscoelastic shell

Various studies (e.g., *Giggenbach*, 1995; *Bégué et al.*, 2017) have quantified a magmatic fluid signature in TVZ geothermal waters. If fluids originate from shallow magma bodies, then to become entrained in the geothermal flow, they must first migrate across the viscoelastic shell. The principle difficulty with this is that high temperatures within the shell, which promote viscoelastic deformation of rock, should tend to seal off any permeability. On the other hand, fluids in the magma body are likely to be lithostatically pressured or higher, which would tend to aid tensile fracturing as a means of generating transient permeability.

To model the leakage of magmatic water into overlying geothermal systems, we assume a simple model of a compressible fluid in steady, 1D Darcy flow. Conservation of mass for a control volume within the shell requires:

$$\frac{d}{dz}(\rho_g' v) = 0, \quad (24)$$

where v is the Darcy velocity, i.e., $v = -\frac{k k_r}{\eta_g}\frac{dP'}{dz}$ with k the shell permeability, k_r the relative permeability, η_g the viscosity of water, and P' the fluid pressure in the shell. We set $k_r = \epsilon_g$, which ensures that water leakage drops to zero as the magma dries out. Density of water in the shell, ρ_g', is approximated by a linear compressibility relation:

$$\rho_g' = \rho_g + \frac{1}{\beta_g'}(P' - P_0), \quad (25)$$

where β_g' is the bulk modulus (note, use of primed variables is to distinguish shell quantities from equivalent unprimed quantities in the magma body).

For boundary conditions, (z_{mb}, P) and (z_{BDT}, P_{BDT}), where $P_{BDT} = \rho_d z_{BDT} g$ is the pressure of a cold hydrostatic water column at the BDT, the solution to Eq. (24) is:

$$P' = P - \beta_g' \rho_g + \sqrt{\left(\beta_g' \rho_g\right)^2 + z' \Delta P \left(\Delta P - 2\beta_g' \rho_g\right)}, \quad (26)$$

where $z' = (z - z_{mb})/(z_{BDT} - z_{mb})$ and $\Delta P = P - P_{BDT}$.

At steady-state, conservation of energy through the shell is expressed as the sum of conductive and advective heat flows:

$$K\frac{d^2T'}{dz^2} + c_g \frac{d}{dz}\left(\rho_g' v T'\right) = 0, \quad (27)$$

where c_g is the specific heat and K the thermal conductivity. Using the expression for P' in Eq. (26), we can solve (27) subject to the boundary conditions (z_{mb}, T) and (z_{BDT}, T_{BDT}) to obtain:

$$T' = T - \Delta T \frac{1 - e^{-C(z - z_{mb})}}{1 - e^{-C(z_{BDT} - z_{mb})}}, \quad (28)$$

where $C = -c_g k \epsilon_g \Delta P (2\beta'_g \Delta P - \rho_g)/(K \eta_g (z_{BDT} - z_{mb}))$. For small values of C, the temperature gradient is approximately linear, as conceptualised in Sections 2.2.

From expressions (26) and (28) we can derive the heat loss from the magma body by conduction and fluid leakage:

$$\dot{H}_{cool} = -AK \left. \frac{dT'}{dz} \right|_{z=z_{mb}} \quad (29)$$

$$\dot{M}_{leak} = -A \frac{k \epsilon_g \rho_g}{\eta_g} \left. \frac{dP'}{dz} \right|_{z=z_{mb}} \qquad \dot{H}_{leak} = c_g T \dot{M}_{leak} \quad (30)$$

Note, this analysis neglects both the temperature dependence of the density, and the pressure and temperature dependence of viscosity and specific heat. However, variation over these properties is smaller than the fluid compressibility effect that is approximately captured. In future work, we aim to address this shortcoming through full numerical simulation of the problem.

An alternative model for degassing was recently developed by *Parmigiani et al.* (2017), who used the Lattice-Boltzmann method to investigate volatile flow at different crystal fractions. Those authors then derived approximate relations for absolute and relative permeability, parameterised in terms of crystal fraction, ϵ_X.

3. MODEL APPLICATION

To develop an intuition for the model physics, here we consider a rhyolitic magma body with some generic properties, subject to a constant mass recharge, $\dot{M}_{in}$. The magma body is buried at a depth of 4.5 km, has an initial volume of 100 km^3, and a thickness of 1.5 km (for the assumed sill geometry, this corresponds to a lateral diameter of 9 km). The initial magma composition comprises 4 wt % water and 36 wt % crystals at 800°C. For a full list of model parameters, see Table 1 (Appendix B).

3.1 Eruption triggers

For the first 0.9 kyr, pressure in the magma body increases linearly, an elastic response to constant mass recharge (Fig. 3). When overpressure reaches 20 MPa, a dike eruption is triggered ($\Delta P = \Delta P_{cd}$). Rapid removal of mass during the eruption causes pressure to drop back to lithostatic, at which point slow pressure rise due to recharging magma resumes.

A second eruption occurs at 1.8 kyr and a third at 2.7 kyr, i.e., eruptions are regularly spaced at a timescale governed by elastic cycling parameters ($\dot{M}_{in}$, β_r, and ΔP_{cd}). The fourth and subsequent eruptions are triggered at successively smaller overpressures, and hence successively shorter times between events. This is due to evolution of the magma content, in particular, the abrupt increase in exsolved water that occurs during the eruptive phase of pressure drop and boiling (Fig. 3). This in turn affects the fragmentation eruption criterion, $\Delta P_{cf} = 10^6/\epsilon_g$ (*Spieler et al.*, 2004), which is now satisfied at a lower overpressure than the dike propagation criterion ($\Delta P = \Delta P_{cf}$).

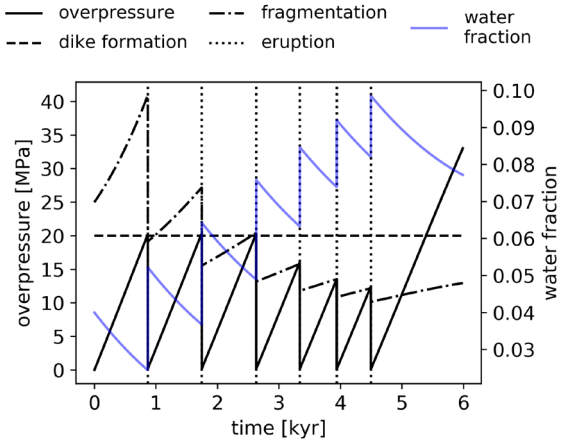

Figure 3: Evolution of pressure (black) and magmatic water content (blue) over 6 kyr and six eruptions. Eruptions are indicated by dotted lines and abrupt changes in physical parameters. Diking and fragmentation eruption criteria are indicated by dashed and dah-dotted lines.

3.2 Cooling and locking

Juxtaposed against the cyclic pressure evolution is a long-term thermal evolution of the magma body (Fig. 4). Temperature declines steadily between eruptions at about 4 or 5°C kyr^{-1}. Temperature drops much more rapidly *during* an eruption for two reasons. First, the abrupt drop in pressure causes water to exsolve from the melt, a process that absorbs heat. Second, the exsolved water has a *higher* specific heat capacity than the melt and crystal components; the same quantity of sensible heat will exist at a lower temperature in the wetter mixture. In future treatments, it may be important to consider variation of the specific heat capacity with both temperature and dissolved water fraction (e.g., *Bouhifd et al.*, 2013), so as to improve the cooling calculation

The trend in crystallinity, inverse to the thermal evolution, reflects the strong temperature dependence of the melting curve (Eq. 38). When crystallinity exceeds 50%, shortly after the sixth eruption, the magma body locks up and becomes non-eruptible.

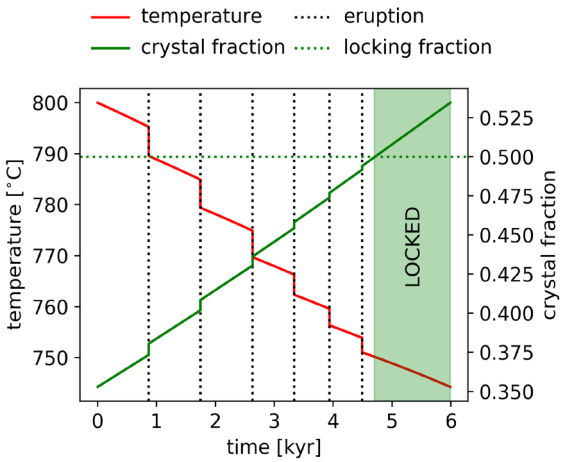

Figure 4: Evolution of temperature (red) and crystal fraction, ϵ_X (green). The magma body becomes locked and non-eruptible when $\epsilon_X > 0.5$, which occurs after the sixth eruption.

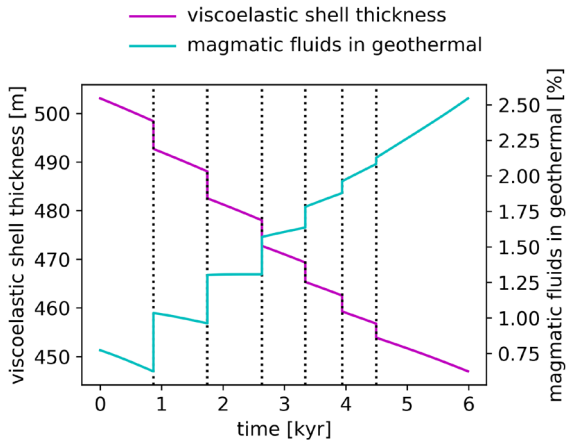

Figure 5: Viscoelastic shell thickness (purple) and magmatic fluid leakage (cyan) as a percentage of the overlying geothermal upflow.

3.3 Overlying geothermal systems

Rapid cooling of the magma body is driven by the parameterised model of overlying geothermal convection. Eq. (18) summarises the trade-off between geothermal dissipation, γ, and magmatic heat supply, T, which determines the thickness of an intermediate viscoelastic zone separating the magma body from the permeable, brittle crust. As temperature drops from 800°C to 750°C, the viscoelastic zone thins from 500 to 450 m thick (Fig. 5).

Although we have prescribed a relatively low permeability in the viscoelastic zone, 10^{-20} m^2, the immense pressure gradient across it nevertheless drives an appreciable rate of magmatic fluid loss. For rainfall rates and infiltration similar to the TVZ, the escaped fluids contribute up to 2% of the total geothermal upflow. The average geothermal heat flux above the magma body is 2.4 W m^{-2}.

3.4 Other observables

Erupted volume is computed by integrating the mass efflux rate ($\dot{M}_{erupt}$ = 10^7 kg s^{-1}) over the erupting period and dividing by the mixture density. The first three eruptions produce about 2.8 km^3 (Fig. 6), of which about 4 to 6% is magmatic water (Fig. 3). Subsequent eruptions are smaller,

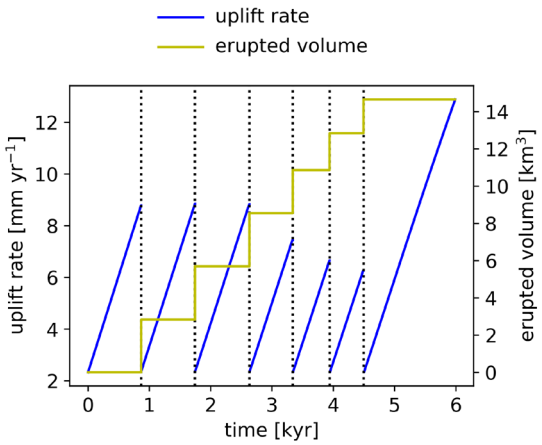

Figure 6: Cumulative erupted volume (yellow) over the course of six modelled eruptions. Also plotted is the uplift rate (blue) between eruptions, assuming a 1D column model.

because the pressure build-up (and hence mass loss to dissipate the overpressure) is less.

Because the magma body is being recharged from a deeper source, its volume increases between eruptions. In the limit that this new volume is accommodated by purely vertical displacement, then we can approximate the surface uplift rate:

$$\frac{dw}{dt} = \frac{1}{A}\frac{dV}{dt}. \qquad (31)$$

For this model, uplift rate is between 2 and 9 mm/yr, increasingly linearly in the period between eruptions. This suggests that the dominant volumetric response is viscoelastic (proportional to ΔP, the second term on the RHS of Eq. 6) rather than elastic (proportional to dP/dt).

4. APPLICATION TO MODERN TVZ

The eruptive history of the TVZ is complex, with the locus of activity over the last 2 million years jumping between different volcanic centres (*Wilson and Rowland*, 2016). In this study, we will restrict our attention to the most recent 30 kyr of activity, for which *Lowe et al.* (2013) have provided a detailed eruption history. During this time, there were 21 eruptions from two primary volcanic centres – Taupō and Okataina – approximately one eruption per centre every 3000 years. In terms of total erupted volume, the record is dominated by the 26.5 ka Oruanui eruption, which generated 530 km^3. The other eruptions averaged about 7 km^3 (the 1.8 ka Taupō eruption produced about 35 km^3).

Studies of quartz-hosted melt inclusions frozen in TVZ erupted products record the pressure conditions in which they formed (*Bégué et al.*, 2014b). These indicate that many rhyolitic magma bodies existed at shallow depths of 4 to 5 km prior to eruption.

Efforts to replicate this eruptive style using a model with constant magma recharge, $\dot{M}_{in}$, were largely unsuccessful. For a range of initial volumes (100 to 1000 km^3), thicknesses (1 to 2.5 km), and geothermal efficiency (5 to 15), the magma body would always cool and lock up after 10 kyr having only produced a handful of eruptions. Increasing $\dot{M}_{in}$ enough to counteract cooling of the magma body resulted in eruptions that were either too large, or much too frequent.

However, there is no reason to believe deep recharge should be constant in time. For instance, *Allan et al.* (2013) showed from crystals preserved in the 26.5 ka Oruanui eruption products that the eruptible body may have been assembled in only a few hundred years. This suggests the magma body could have existed as a cool mush for long periods, before being rapidly heated prior to eruption (cf. cold storage and rapid heating from sporadic magma recharge for the 0.7 ka Kaharoa TVZ eruption; *Rubin et al.*, 2017). Using their thermomechanical model, *Degruyter et al.* (2016) explored the effect of both rate and duration of transient recharge events. They showed that the recharge event must be both rapid enough to overcome viscoelastic stress dissipation and large enough to generate eruptive overpressure.

In an attempt to replicate the sporadic nature of the modern TVZ eruptive record, we have implemented a stochastic transient recharge model. The i^{th} magma recharge event is modelled as a Gaussian distribution:

$$\dot{M}_{in}^{(i)}(t) = \frac{\Delta M_i}{\delta t\sqrt{2\pi}} \exp\left(-\frac{1}{2}\left(\frac{t-t_i}{\delta t}\right)^2\right), \quad (32)$$

where δt is the duration of the event (100 yrs), t_i is the time it occurs, and ΔM_i is the total mass injected during the event. A continuous, differentiable recharge rate is then constructed as the sum over N recharge events.

The timing of recharge events are modelled as Poissonian, which is enforced by drawing interevent times, $\Delta t_i = t_{i+1} - t_i$, from an exponential distribution with rate parameter, λ:

$$P(\Delta t) = \lambda \exp(-\lambda \Delta t). \quad (33)$$

The size of each recharge event is drawn from a lognormal distribution, with mean, μ, scale, σ, and shape parameter, s:

$$P(\Delta M) = \frac{1}{s\Delta M\sqrt{2\pi}} \exp\left(-\frac{1}{2}\left(\frac{\log(\Delta M - \mu) - \sigma}{\mathrm{s}}\right)^2\right). \quad (34)$$

A model constructed on these principles is presented in Fig. 7. Parameters values for this model are given in Table 2 of Appendix B.

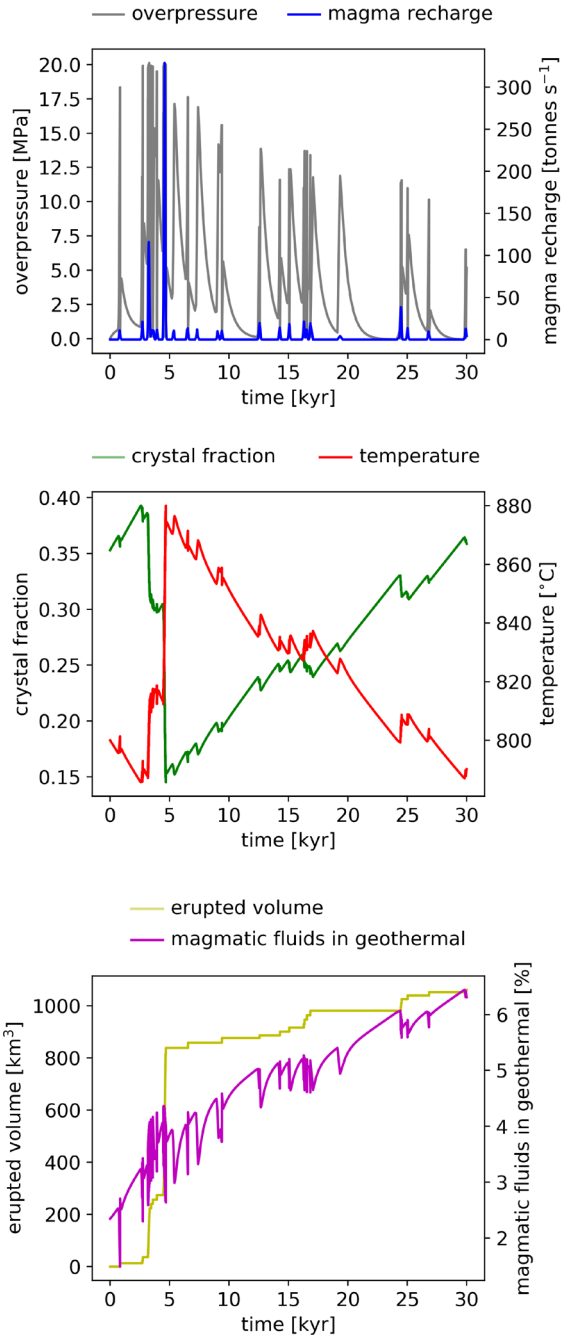

Figure 7: Time evolution of magma and geothermal system properties for a Modern TVZ-like model with sporadic magma recharge. This particular realization is dominated by two large eruptions early on, and smaller eruptions subsequently.

An early phase of high-rate magma recharge results in a series of large eruptions over a short span of time (Fig. 7). Following this period, the magma body has been primed (heated) such that smaller episodes of recharge will trigger small eruptions. Eventually, the magma body would cool and crystallise sufficiently that it becomes locked, after which no further small eruptions would occur. Another large recharge event would be required to transition the magma body back to a higher temperature, eruptible state.

About 14 eruptions occur during the 30 kyr period, although several of these would be better characterised as prolonged eruptive phases. The total erupted mass is about 60% larger than from the TVZ over a similar time period, although given the stochastic nature of our recharge model, an order of magnitude agreement is sufficient.

The proportion of magmatic water leaking into the overlying geothermal systems increases from 2 to 6%. This is consistent with observations (*Giggenbach*, 1995; *Bégué et al.*, 2017), if somewhat on the low side.

5. CLIMATICALLY MODULATED VOLCANISM?

Earlier, we alluded to the possibility that TZV rainfall, $\dot{R}$, which in turn drives the rate of convective geothermal cooling, could vary over glacial-interglacial cycles. Given the coupling between geothermal and magmatic systems, modulation of one may affect modulation of the other. For example, 12 out of the 15 large eruptions to have occurred in the TVZ in the past 1.2 million years did so during glacial periods (*Allan et al.*, 2008).

To test this idea, we modify the models described in Sections 4 and 5 to include a simple sinusoidal modulation of the geothermal power multiplier, γ, i.e.:

$$\gamma(t) = \gamma_0 + \Delta\gamma \sin(\omega t) \quad (35)$$

where γ_0, $\Delta\gamma$ and ω are the base value, amplitude and frequency of modulation. Such modulation and the corresponding eruption records are presented in Fig. 8, alongside unmodulated benchmarks.

In the first instance, we have applied almost the largest possible modulation to the generic eruption model (constant $\dot{M}_{in}$) from Section 4. This results in several of the eruptions occurring a few hundred years earlier than they otherwise would, although no strong correlation between geothermal power and eruptions is apparent. A relation between the two is even less likely when applying a plausible modulation – 25% variability of the rainfall rate – to the TVZ-like eruption model.

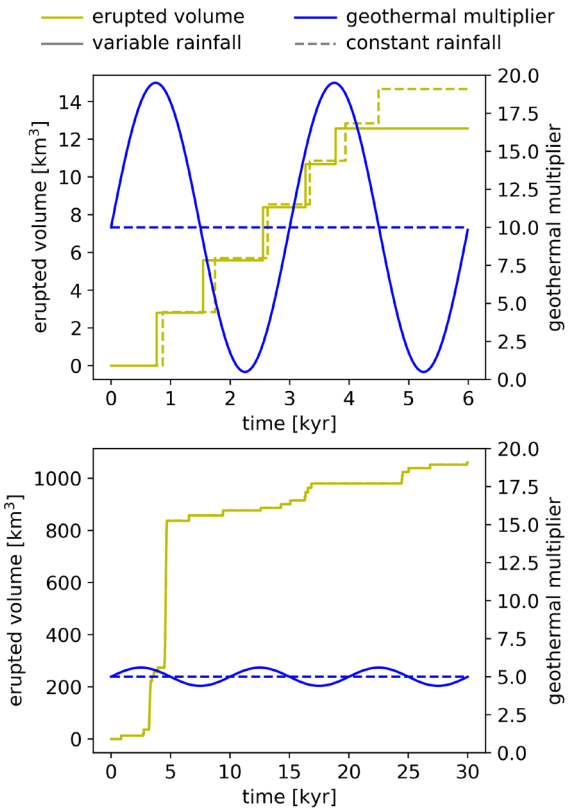

Figure 8: Comparison between modelled eruption records (yellow) with and without modulation (solid and dashed) of the geothermal power multiplier (blue). The models correspond to the generic eruption model in Section 3 (top) and the TVZ-like model in Section 4 (bottom).

6. GEOTHERMALLY TRIGGERED ERUPTIONS

It is not just deep magma recharge, sporadic or otherwise, that can drive overpressure and trigger an eruption. *Tramontano et al.* (2017) modelled the conditions under which silicic magma bodies could erupt through internal changes: volatile exsolution and crystallisation during cooling. Here, we also test the concept of internally triggered eruptions, allowing also for elevated geothermal cooling, magma degassing (leakage of magmatic water across the viscoelastic shell) and viscous stress dissipation.

We consider again the generic eruption model (Section 3 and Table 1) modified only to exclude the source of magma recharge, i.e., $\dot{M}_{in}$= 0. We then model cooling of the magma body by either strong (γ = 10) or weak (γ = 5) geothermal systems (Fig. 9).

As the modelled magma body cools, the solubility of water in the melt decreases. Subsequent exsolution of the water increases internal pressure. For the case of strong geothermal cooling, this internal evolution occurs over sufficiently short timescales that neither viscoelastic dissipation nor degassing can prevent an eruption occurring. This is not the case for the model with weak geothermal cooling; overpressure plateaus before an eruption is triggered.

To demonstrate the controlling influence of viscous dissipation and magma degassing, we have also modelled cases of strong geothermal cooling with elevated degassing (k = 10^{-19} m^2) or a less viscous shell (η_r = 5×10^{-19} Pa s).

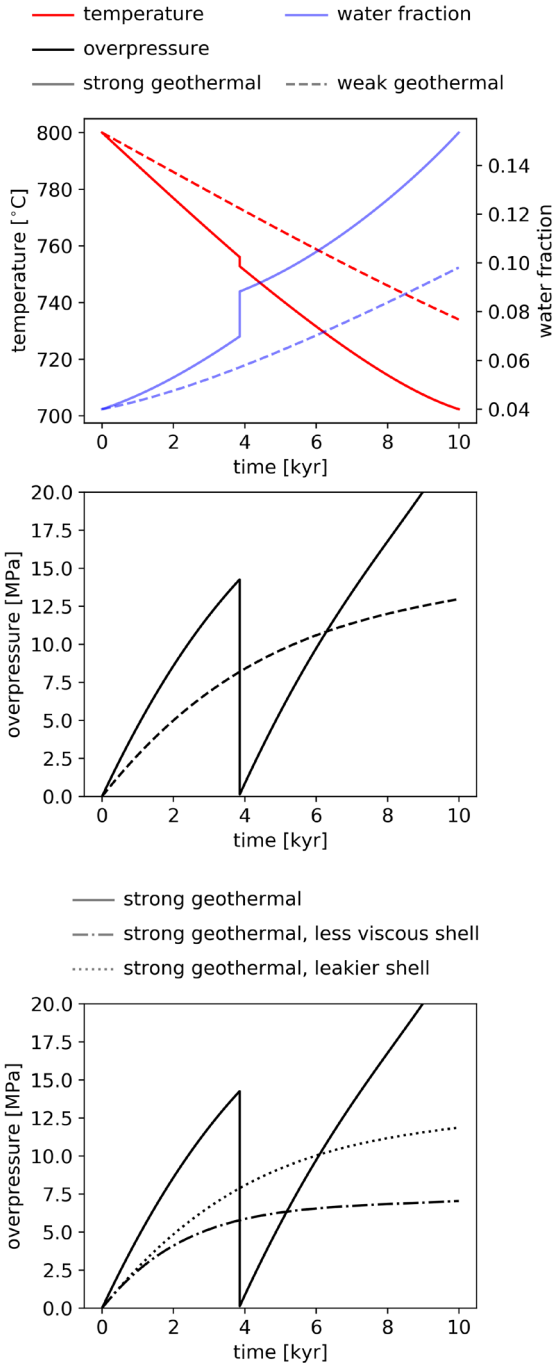

Figure 9: Evolution of a magma body under strong (solid, γ = 10) and weak (dashed, γ = 5) geothermal cooling, and for efficient degassing (dotted, γ = 10) or a weak viscous shell (dash-dot, γ = 10).

Both conditions are sufficient to prevent an eruption from occurring.

7. SUMMARY AND FUTURE QUESTIONS

We have introduced a lumped parameter model for the evolution of pressure, temperature, and volume of a silicic magma body comprising a mixture of water, melt and crystals. Our model accounts for phase change and water exsolution, heat and mass loss by geothermally enhanced cooling, leakage of water, and sporadic eruptions, and viscoelastic stress evolution. For certain parameter combinations, the model replicates several features of TVZ

volcanism and geothermal expression, including approximate eruptive volumes and frequencies, and magmatic fluid contribution to geothermal upflow.

Our findings suggest that short, sporadic episodes of deep magma recharge are adequate to explain observations of rapid assembly and eruption from shallow depths. Although geothermal cooling plays an important role in transitioning magma bodies to a cooler, non-eruptible state, plausible fluctuations in geothermal power (due, say, to climatically driven variations in the rainfall rate) have no impact on eruption timing. However, where the overlying geothermal systems are sufficiently powerful (and both degassing and viscous dissipation are small), this coupling can drive water exsolution within the magma leading to an eruption.

In undertaking this study, we identified several shortcomings of the modelling approach that could be addressed in future work. The lumped parameter nature of the model prohibits any investigation spatial variability – of pressure, temperature, crystallinity, etc. – either laterally or with depth within the magma body. Although we have considered here a sill geometry, the viscoelastic term in Eq. (**6**) is really only appropriate for a spherical magma body (however, we imagine it should be correct to within an order of magnitude). Finally, our parameterisation of the geothermal systems, including determination of the BDT depth, assumes the magmatic and geothermal systems are in equilibrium. However, during periods of rapid change (an eruption), the system should experience temporary periods of considerable disequilibrium. Addressing these, and other, shortcomings could be achieved through development of a multidimensional simulator for multi-phase (water/steam, melt/crystals), multi-component (water and rock) heat and mass transfer, with equations of state defined for extreme temperatures and pressures, and ideally incorporating a viscoelastic mechanical model.

ACKNOWLEDGEMENTS

The authors thank Mike O'Sullivan for help solving the viscoelastic shell flow equations.

APPENDIX A

A.1 Equations of state

The density of free phase supercritical water in the magmatic mixture is given by *Huber et al.* (2010):

$$\rho_g = 10^3(-112.528T^{-0.381} + 127.811P^{-1.135} + 112.04T^{-0.411}P^{0.033}), \quad (36)$$

where T is in °C and P is in bar.

The solubility of water in melt uses the parameterisation of *Dufek and Bergantz* (2005):

$$m_{eq} = 10^{-2}\left(P^{0.5}\left(0.4874 - \frac{608}{T} + \frac{489530}{T^2}\right) + P\left(-0.06062 + \frac{135.6}{T} - \frac{69200}{T^2}\right) + P^{1.5}\left(0.00253 - \frac{4.154}{T} + \frac{1509}{T^2}\right)\right), \quad (37)$$

where P is in MPa and T is in Kelvin.

The crystal fraction (melting curve) is given by the parameterisation of *Huber et al.* (2010):

$$\epsilon_X = (1-\epsilon_g)\left(1 - \left(\frac{T-T_s}{T_l-T_s}\right)^b\right), \quad (38)$$

where T_s and T_l are solidus and liquidus temperatures, and b = 0.5 for silicic magmas.

A.2 Governing equations

Equations here replicate those in *Degruter and Huber* (2014) with minor modifications for a leaky viscoelastic shell.

Coefficients for the mass conservation equation:

$$\begin{aligned} A_m &= -\left(\frac{1}{\beta} + \frac{1}{\beta_r}\right), \\ B_m &= -\left(-\alpha - \alpha_r + \frac{\rho_X - \rho_m}{\rho}\frac{\partial \epsilon_X}{\partial T}\right), \\ C_m &= -\left(\frac{\rho_g - \rho_m}{\rho} + \frac{\rho_X - \rho_m}{\rho}\frac{\partial \epsilon_X}{\partial \epsilon_g}\right), \\ D_m &= \frac{\dot{M}_{in} - \dot{M}_{erupt} - \dot{M}_{leak}}{\rho V} - \frac{\Delta P}{\eta_r}, \end{aligned} \quad (39)$$

where we have defined an effective bulk modulus and thermal expansion coefficient for the mixture:

$$\begin{aligned} \frac{1}{\beta} &= \frac{1}{\rho}\left(\epsilon_m\frac{\rho_m}{\beta_m} + \epsilon_X\frac{\rho_X}{\beta_X} + \epsilon_g\frac{\partial \rho_g}{\partial P}\right), \\ \alpha &= \frac{1}{\rho}\left(\epsilon_m\rho_m\alpha_m + \epsilon_X\rho_X\alpha_X - \epsilon_g\frac{\partial \rho_g}{\partial T}\right). \end{aligned} \quad (40)$$

Coefficients for the water conservation equation:

$$\begin{aligned} A_w &= -\left(\frac{1}{\rho_g}\frac{d\rho_g}{dP} + \frac{1}{\beta_r} + \frac{m_{eq}\rho_m\epsilon_m}{\rho_g\epsilon_g}\left[\frac{1}{m_{eq}}\frac{\partial m_{eq}}{\partial P} + \frac{1}{\beta_m} + \frac{1}{\beta_r}\right]\right), \\ B_w &= -\left(\frac{1}{\rho_g}\frac{d\rho_g}{dT} - \alpha_r + \frac{m_{eq}\rho_m\epsilon_m}{\rho_g\epsilon_g}\left[\frac{1}{m_{eq}}\frac{\partial m_{eq}}{\partial T} - \alpha_m - \alpha_r - \frac{1}{\epsilon_m}\frac{\partial \epsilon_X}{\partial T}\right]\right), \\ C_w &= -\left(\frac{1}{\epsilon_g} - \frac{m_{eq}\rho_m}{\rho_g\epsilon_g}\left[1 + \frac{\partial \epsilon_X}{\partial \epsilon_g}\right]\right), \\ D_w &= \frac{\dot{M}_{w,in} - \dot{M}_{w,erupt} - \dot{M}_{w,leak}}{\rho_g\epsilon_g V} - \frac{\Delta P}{\eta_r}\left(1 + \frac{m_{eq}\rho_m\epsilon_m}{\rho_g\epsilon_g}\right). \end{aligned} \quad (41)$$

Coefficients for the energy conservation equation:

$$\begin{aligned} A_h &= -\left(\frac{1}{\beta} + \frac{1}{c}\frac{\partial c}{\partial P} + \frac{1}{\beta_r} - \frac{L_m\rho_X\epsilon_X}{\rho cT}\left[\frac{1}{\beta_X} + \frac{1}{\beta_r}\right] - \frac{L_e m_{eq}\rho_m\epsilon_m}{\rho cT}\left[\frac{1}{m_{eq}}\frac{\partial m_{eq}}{\partial P} + \frac{1}{\beta_m} + \frac{1}{\beta_r}\right]\right), \\ B_h &= -\left(-\alpha + \frac{\rho_X - \rho_m}{\rho}\frac{\partial \epsilon_X}{\partial T} + \frac{1}{c}\frac{\partial c}{\partial T} + \frac{1}{T} - \alpha_r - \frac{L_m\rho_X\epsilon_X}{\rho cT}\left[-\alpha_X + \frac{1}{\epsilon_X}\frac{\partial \epsilon_X}{\partial T} - \alpha_r\right] - \frac{L_e m_{eq}\rho_m\epsilon_m}{\rho cT}\left[\frac{1}{m_{eq}}\frac{\partial m_{eq}}{\partial P} - \alpha_m - \frac{1}{\epsilon_m}\frac{\partial \epsilon_X}{\partial T} - \alpha_r\right]\right), \\ C_h &= -\left(\frac{\rho_g - \rho_m}{\rho} + \frac{\rho_X - \rho_m}{\rho}\frac{\partial \epsilon_X}{\partial \epsilon_g} + \frac{1}{c}\frac{\partial c}{\partial \epsilon_g} - \frac{L_m\rho_X}{\rho cT}\frac{\partial \epsilon_X}{\partial \epsilon_g} + \frac{L_e m_{eq}\rho_m}{\rho cT}\left[1 + \frac{\partial \epsilon_X}{\partial \epsilon_g}\right]\right), \\ D_h &= \frac{\dot{H}_{in} - \dot{H}_{erupt} - \dot{H}_{cool} - \dot{H}_{leak}}{\rho cTV} - \frac{\Delta P}{\eta_r}\left(1 - \frac{L_m\rho_X\epsilon_X}{\rho cT} - \frac{L_e m_{eq}\rho_m\epsilon_m}{\rho cT}\right), \end{aligned} \quad (42)$$

where the partial derivatives of the specific heat are:

$$\begin{aligned} \frac{\partial c}{\partial P} &= \frac{1}{\rho}\left(\frac{\rho_X\epsilon_X c_X}{\beta_X} + \epsilon_g c_g\frac{\partial \rho_g}{\partial P} + \frac{\rho_m\epsilon_m c_m}{\beta_m}\right) - \frac{c}{\rho}\frac{\partial \rho}{\partial P}, \\ \frac{\partial c}{\partial T} &= \frac{1}{\rho}\left(-\alpha_X\rho_X\epsilon_X c_X + \epsilon_g c_g\frac{\partial \rho_g}{\partial T} - \alpha_m\rho_m\epsilon_m c_m\right) - \frac{c}{\rho}\frac{\partial \rho}{\partial T} + \left(\frac{\rho_X c_X - \rho_m c_m}{\rho} - \frac{c}{\rho}\frac{\partial \rho}{\partial \epsilon_X}\right)\frac{\partial \epsilon_X}{\partial T}, \\ \frac{\partial c}{\partial \epsilon_g} &= \frac{\rho_g c_g - \rho_m c_m}{\rho} - \frac{c}{\rho}\frac{\partial \rho}{\partial \epsilon_g} + \left(\frac{\rho_X c_X - \rho_m c_m}{\rho} - \frac{c}{\rho}\frac{\partial \rho}{\partial \epsilon_X}\right)\frac{\partial \epsilon_X}{\partial \epsilon_g}. \end{aligned} \quad (43)$$

APPENDIX B

Table 1: Model parameters for the generic system. All values from *Degruyter and Huber* (2014) unless indicated.

Magma body		*Viscoelastic shell*	
α_m	10^{-5} K^{-1}	α_r	10^{-5} K^{-1}
α_X	10^{-5} K^{-1}	β_r	10^{10} Pa
b	0.5	g	9.81 m s^{-2}
β_m	10^{10} Pa	K	2.5 W m^{-1} K^{-1}
β_X	10^{10} Pa	η_g	5.2×10^{-5} Pa s
c_m	1.2 kJ kg^{-1} K^{-1} (3)	η_r	10^{20} Pa s
c_X	1.3 kJ kg^{-1} K^{-1} (3)	ρ_r	2600 kg m^{-3}
c_g	3.9 kJ kg^{-1} K^{-1} (3)		
L_e	6.1×10^{5} J kg^{-1} (3)	*Geothermal system*	
L_m	2.9×10^{5} J kg^{-1} (3)	γ	10
$\dot{M}_{in}$	200 kg s^{-1}	ϵ	0.02 (2)
$\dot{M}_{erupt}$	10^{7} kg s^{-1}	k	10^{-19} m^2
P_{lith}	$\rho_r g z_{mb}$	ρ_d	1000 kg m^{-3}
ΔP_{cd}	20 MPa	q_{fld}	7.6×10^{7} kg m^{-2}s^{-1}
T_l	950°C	$\dot{R}$	3.8×10^{-8} m s^{-1}
T_s	700°C	T_{atm}	25°C
Initial conditions		*Geometry*	
P_i	P_{lith}	T_{BDT}	350°C
T_i	800°C (1)	Δz	1000 m
$\epsilon_{g,i}$	0.04	z_{mb}	4500 m
$\rho_{m,i}$	2400 kg m^{-3}		
$\rho_{X,i}$	2600 kg m^{-3}		
V_i	100 km^3 (1)		

(1) *Bégué et al.* (2014a)
(2) *Kissling and Weir* (2005)
(3) *Caricchi and Blundy* (2015)

Table 2: TVZ model parameters. All values are the same as Table 1 unless listed below.

Magma recharge		*Viscoelastic shell*	
λ	0.67 kyr^{-1}	η_r	10^{19} Pa s
μ	4.2×10^{13} kg		
σ	2.6×10^{12} kg	*Geothermal system*	
s	3	γ	5
δt	100 yr	k	5×10^{-19} m^2
Initial conditions		*Geometry*	
V_i	500 km^3	Δz	1500 m

REFERENCES

Allan A. S. R., J. A. Baker, L. Carter, and R. J. Wysoczanksi. *Reconstructing the Quaternary evolution of the world's most active silicic volcanic system: insights from an ~1.65 Ma deep ocean tephra record source from the Taupo Volcanic Zone, New Zealand.* Quaternary Science Reviews 27, 2341-2360 (2008).

Allan, A. S. R., D. J. Morgan, C. J. N. Wilson, and M.-A. Millet. *From mush to eruption in centuries: assembly of the super-sized Oruanui magma body.* Contributions to Mineral Petrology 166, 143-164 (2013).

Arehart, G. B., B. W. Christenson, C. P. Wood, K. A. Foland, and P. R. L. Browne. *Timing of volcanic, plutonic and geothermal activity at Ngatamariki, New Zealand.* Journal of Volcanology and Geothermal Research 116, 201-214 (2002).

Bégué, F., C. D. Deering, D. M. Gravley, B. M. Kennedy, I. Chambefort, G. A. Gualda, and O. Bachmann. *Extraction, Storage and Eruption from Multiple Isolated Magma Batches in the Paired Mamaku and Ohakuri Eruption, Taupo Volcanic Zone, New Zealand*. Journal of Petrology 55, 1653-1684 (2014a).

Bégué, F., G. A. R. Gualda, M. S. Ghiorso, A. S. Pamukcu B. M. Kennedy, D. M. Gravley, C. D. Deering, and I. Chambefort. *Phase-equilibrium geobarometers for silicic rocks based on rhyolite-METLS. Part 2: application to Taupo Volcanic Zone rhyolites*. Contributions to Mineral Petrology 168, (2014b).

Bégué, F., C. D. Deering, D. M. Gravley, I. Chambefort, and B. M. Kennedy. *From source to surface: Tracking magmatic boron and chlorine input into the geothermal systems of the Taupo Volcanic Zone, New Zealand*. Journal of Volcanology and Geothermal Research 346, 141-150 (2017).

Bibby, H. M., T. G. Caldwell, F. J. Davey, and T. H. Webb. *Geophysical evidence on the structure of the Taupo Volcanic Zone and its hydrothermal circulation.* Journal of Volcanology and Geothermal Research 68, 29-58 (1995).

Bouhifd, M. A., A. G. Whittington, A. C. Withers, and P. Richet. *Heat capacities of hydrous silicate glasses and liquids*. Chemical Geology 346, 125-134 (2013).

Bryan, C. J., S. Sherburn, H. M. Bibby, S. C. Bannister, and A. W. Hurst. *Shallow seismicity of the central Taupo Volcanic Zone, New Zealand: its distribution and nature.* New Zealand Journal of Geology and Geophysics 42, 533-542 (1999).

Caricchi, L., and J. Blundy. *Experimental petrology of monotonous intermediate magmas*. Geological Society Special Publications 422, 105-130 (2015).

Degruyter, W, and C. Huber. *A model for eruption frequency of upper crustal silicic magma chambers.* Earth and Planetary Science Letters 403, 117-130 (2014).

Degruyter, W., C. Huber, O. Bachmann, K. M. Cooper, and A. J. R. Kent. *Magma reservoir response to transient recharge events: The case of Santorini volcano (Greece)*. Geology 44, 23-26 (2016).

Dempsey, D. E., S. F. Simmons, R. A. Archer, and J. V. Rowland. *Delineation of catchment zones of geothermal systems in large-scale rifted settings.* Journal of Geophysical Research 117, doi: 10.1029/2012JB009515 (2012).

Dufek, J., and G. W. Bergantz. *Transient two-dimensional dynamics in the upper conduit of a rhyolitic eruption: a comparison of closure models for the granular stress.* Journal of Volcanology and Geothermal Research 143, 113-132 (2005).

Eaves, S.R., A. N. Mackintosh, B. M. Anderson, A. M. Doughty, D. B. Townsend, C. E. Conway, G. Winckler, J. M. Schaefer, G. S. Leonard, and T. A. Calvert. *The Last Glacial Maximum in the central North Island, New Zealand: palaeoclimate inferences from glacier modelling*. Climates of the Past 12, 943-960 (2016).

Giggenbach, W. F. *Variations in the chemical and isotopic composition of fluids discharged from the Taupo Volcanic Zone, New Zealand*. Journal of Volcanology and Geothermal Research 68, 89-116 (1995).

Hochstein, M. P. *Crustal heat transfer in the Taupo Volcanic Zone (New Zealand): comparison with other volcanic arcs and explanatory heat source models*. Journal of Volcanology and Geothermal Research 68, 117-151 (1995).

Huber, C., O. Bachmann, and M. *Manga Two Competing Effects of Volatiles on Heat Transfer in Crystal-rich Magmas: Thermal Insulation vs Defrosting*. Journal of Petrology 51, 847-867 (2010).

Jellinek, A. M., and D. J. DePaolo. *A model for the origin of large silicic magma chambers: precursors of caldera-forming eruptions*. Bulletin of Volcanology 65, 363-381 (2003).

Kissling, W. M., and G. J. Weir. *The spatial distribution of the geothermal fields in the Taupo Volcanic Zone, New Zealand*. Journal of Volcanology and Geothermal Research 145, 136-150 (2005).

Kissling, W., S. Ellis, F. Charpentier, and H. Bibby. *Convective flows in a TVZ-like setting with a brittle/ductile transition.* Transport in Porous Media 77, 335-355 (2009).

Kissling, W., and S. Ellis. *Modelling the flow of hydrothermal fluids above an evolving continental rift.* Proceedings of the 31st New Zealand Geothermal Workshop, Rotorua (2009).

Lowe, D. J., M. Blaauw, A. G. Hogg, and R. M. Newnham. *Ages of 24 widespread tephras erupted since 30,000 years ago in New Zealand, with re-evaluation of the timing and palaeoclimatic implications of the Lateglacial cool episode recorded at Kaipo bog.* Quaternary Science Reviews 74, 170-194 (2013).

Parmigiani, A., W. Degruyter, S. Leclaire, C. Huber, and O. Bachmann. *The mechanics of shallow magma reservoir outgassing*. Geochemistry, Geophysics, Geosystems 18, 2887-2905 (2017).

Rubin, A. E., K. M. Cooper, C. B. Till, A. J. R. Kent, F. Costa, M. Bose, D. Gravley, C. Deering, and J. Cole. *Rapid cooling and cold storage in a silicic magma reservoir recorded in individual crystals.* Science 356, 1154-1156 (2017).

Sigmundsson F., V. Pinel, B. Lund, F. Albino, C. Pagli, H. Geirsson, and E. Sturkell. *Climate effects on volcanism: influence on magmatic systems of loading and unloading from ice mass variations, with examples from Iceland*. Philosophical Transactions of the Royal Society A 368, 2519-2534 (2010).

Spieler, O., B. Kennedy, U. Kueppers, D. B. Dingwell, B. Scheu, and J. Taddeucci. *The fragmentation threshold of pyroclastic rocks*. Earth and Planetary Science Letters 226, 139-148 (2004).

Tramontano, S., G. A. R. Gualda, and M. S. Ghiorso. *Internal triggering of volcanic eruptions: tracking overpressure regimes for giant magma bodies*. Earth and Planetary Science Letters 472, 142-151 (2017).

Weir, G. J. *A mathematical model of rainfall-controlled geothermal fields.* Transport in Porous Media 77, 323-334 (2009).

Wilson, C. J. N., and J. V. Rowland. *The volcanic, magmatic and tectonic setting of the Taupo Volcanic Zone, New Zealand, reviewed from a geothermal perspective.* Geothermics 59, 168-187 (2016).